*Published online 3 May 2021*

*NAR Genomics and Bioinformatics, 2021, Vol. 3, No. 2* **1**
*doi: 10.1093/nargab/lqab033*

# Transcription factor allosteric regulation through substrate coordination to zinc

**Beatriz C. Almeida[1], Jennifer A. Kaczmarek[2], Pedro R. Figueiredo[1], Kristala L.J. Prather[2] and Alexandra T.P. Carvalho[1,*]**

[1]CNC—Center for Neuroscience and Cell Biology, Institute for Interdisciplinary Research (IIIUC), University of Coimbra, 3004-504 Coimbra, Portugal and [2]MIT—Department of Chemical Engineering, Massachusetts Institute of Technology, Cambridge, MA 02139, USA

Received November 17, 2020; Revised March 30, 2021; Editorial Decision April 04, 2021; Accepted April 08, 2021

## ABSTRACT

**The development of new synthetic biology circuits for biotechnology and medicine requires deeper mechanistic insight into allosteric transcription factors (aTFs). Here we studied the aTF UxuR, a homodimer of two domains connected by a highly flexible linker region. To explore how ligand binding to UxuR affects protein dynamics we performed molecular dynamics simulations in the free protein, the aTF bound to the inducer D-fructuronate or the structural isomer D-glucuronate. We then validated our results by constructing a sensor plasmid for D-fructuronate in *Escherichia coli* and performed site-directed mutagenesis. Our results show that zinc coordination is necessary for UxuR function since mutation to alanines prevents expression de-repression by D-fructuronate. Analyzing the different complexes, we found that the disordered linker regions allow the N-terminal domains to display fast and large movements. When the inducer is bound, UxuR can sample an open conformation with a more pronounced negative charge at the surface of the N-terminal DNA binding domains. In opposition, in the free and D-glucuronate bond forms the protein samples closed conformations, with a more positive character at the surface of the DNA binding regions. These molecular insights provide a new basis to harness these systems for biological systems engineering.**

## INTRODUCTION

Gammaproteobacteria have a remarkable capability, in stress conditions, to form complexes with regulatory proteins and different molecules, thus, acquiring structural and functional changes, to switch between metabolic pathways to accomplish an overarching purpose (e.g. growth) (1,2). The ability to control regulatory proteins (also named transcription factors: TFs) has been extensively studied, becoming one of the challenges in modern molecular biology. Several TFs are sensitive to small metabolites, ions or drugs, which can modify their binding to DNA, thereby regulating gene expression (2). One mechanism associated with these TFs, enhancing the response to environmental signals, is allosteric regulation (1). TFs that are inducible by small molecules are useful synthetic biology tools as sensors and switches (3).

Bacterial allosteric TFs (aTFs) encompass several families of proteins (1,3). The gluconate operon repressor in *Bacillus subtilis* (GntR) superfamily (Pfam-PF0032) (4) is a large group of TFs present in several bacterial groups (5) and they regulate fundamental biological processes, such as motility (6), development (7), antibiotic production and resistance (8,9), plasmid transfer (10) and virulence (11). Despite the fact that most of the GntR TFs available in the PDB database do not contain metals, some studies strongly suggest that the majority of fatty acid metabolism regulator proteins (FadR) (Pfam-PF07840—the largest family of GntR superfamily) (4) are metal-dependent (1,12–15), However, the underlying allosteric mechanism is poorly understood. It is not clear whether these TFs are metal-sensing, if the metal plays a structural role, or if metals are required for binding of other effector molecules (12–15).

*Escherichia coli* and other Gammaproteobacteria can grow using hexuronic acids as a carbon source (16). This metabolic pathway, named the Ashwell pathway, is controlled by the Uxu operon transcriptional regulator (UxuR TF) (17). UxuR TF represses the expression of its gene (uxuR) and controls the expression of operons that encode the main proteins of the Ashwell pathway (18). Experimental studies indicate that UxuR TF binds to fructuronate (19), the product of the reaction immediately downstream of glucuronate, catalyzed by D-glucuronate/D-galacturonate isomerase in the catabolic pathway. It was shown that fructuronate can influence the interaction of UxuR TF with DNA (19). However, the conformational changes that lead to this transcriptional regulation are

*To whom correspondence should be addressed. Tel: +35 1 231 249 248; Fax: +35 1 231 249 179; Email: atpcarvalho@uc.pt

poorly understood. Previous modeling efforts for UxuR TF assumed that the structure was a monomer or did not consider the hypothesis of metal binding (20,21). Consequently, until now, the ligand-binding site and the residues involved remain unknown, as well as the associated conformational changes.

In this work, we determined and experimentally verified, by site-directed mutagenesis, the ligand-binding site of UxuR TF (homodimer with Zn(II) ion). We furthermore studied the dynamical behavior of UxuR TF, by comparing the unbound structure to structures bound to D-fructuronate and D-glucuronate, independently. Here we have analysed the dynamics and found large NTD domain transitions at the nanosecond range.

## MATERIALS AND METHODS

### Modeling

We resorted to the Rosetta software package for protein structure prediction through the Robetta server (22). A GntR TF from *Streptococcus agalactiae* (23) (PDB code: 6AZ6, 1.91 Å resolution), with 28.9% of identity was used for homology modeling; Regions lacking enough homology, such as the peptide linkers, were modeled using the Rosetta *de novo* structure prediction method.

The zinc metal coordination was modeled using a semi-bonded model approach (cationic dummy atom: CaDA method) according to Pang *et al.* (24,25) The natural ligand, α-D-fructuronate (DFU; PubChem Identifier: CID 46878576) and β-D-glucuronate (GLU; PubChem Identifier: CID 11877136) were obtained from the PubChem Data Base. Both ligands were prepared using the UCSF Chimera program (26) and the parameters were retrieved from the GLYCAM database (27). The atomic partial charges were calculated employing the (RESP) (28) method from the HF/6–31G(d,p) single-point energy calculations.

### Molecular docking

The molecular docking was performed with AutoDock4.2 suite of programs (29) with the Lamarckian Genetic Algorithm (LGA) (30). A grid box (40 × 40 × 40 Å) was centered on the Zn(II) ion, at both chains (chain A: $x = 47.741$; $y =$ -2.039; $z = 21.566$ and chain B: $x = 46.137$; $y = 38.828$; $z =$ 23.538), for DFU as well as for GLU. A total of 100 LGA runs were carried out for each of the ligand–protein complexes. The population was 300, the maximum number of generations was 27 000 and the maximum number of energy evaluations was 2 500 000. All rotatable bonds were kept flexible.

### Molecular dynamics

To study the structural changes between the free protein and complexes with the ligands the proteins were subjected to molecular dynamics (MD) simulations (31–33). MD simulations were performed using the MD software package Amber18 (34) with the parm99SB (35) and GLYCAM06 (27) force fields. The structures were placed in an octahedral box of water molecules (10.0 Å between the surface of the protein to the box). Counter ions were added to make the entire system neutral. Each system was subjected to two initial energy minimizations and 500 ps of equilibration in an NVT ensemble, using Langevin dynamics (36) with small restraints on the protein (10.0 kcal/mol) to heat the systems from 0 K to 310.15 K (optimal temperature for the bacterial organism). Production simulations were carried out at 310.15 K in the NPT ensemble, using Langevin dynamics with a collision frequency of 1 $ps^{-1}$. Constant pressure periodic boundary conditions were imposed with an average pressure of 1 ATM. Isotropic position scaling was used to maintain pressure with a relaxation time of 2 ps. The SHAKE algorithm (37) was applied to all bonds involving hydrogen atoms. The SHAKE feature constrains the vibrational stretching of hydrogen bond lengths and fixes the bond distance to the equilibrium value. The Particle Mesh Ewald method (38) was used to calculate electrostatic interactions with a cutoff distance of 10.0 Å. The total time of the simulations was 2.1 μs (seven replicas with different initial velocities for each situation), the integration time was set to 2 fs.

We performed extensive MD simulations for three situations, intending to better understand the structural conformation change in our aTF: UxuR without any ligand, UxuR with DFU in both chains, and UxuR with GLU in both chains.

### Principal components analysis and free energy landscape

To identify the overall patterns of motions in the three situations, we used principal components analysis (PCA) which was carried out using the CPPTRAJ program (39), comprising 7554 atoms in the free situation and 7598 atoms in the situations with the ligands bound. The trajectories of corresponding atoms were extracted and analyzed for 100 ns using 5 000 000 frames in each replica; the first frame was set as the reference to remove global translation/rotation. The Cartesian covariance matrix of the involved residues was calculated and then diagonalized to provide a series of eigenvectors representing different modes of conformational change and their corresponding eigenvalues. The Bio3d software (40), a package of R software (41), was used to quantify the PCA results. To identify the dominant conformational states, we calculated the free energy landscape (FEL) (42) concerning PC1 and PC2.

The study of conformational transition pathways was performed by the elastic network-driven Brownian Dynamics Importance Sampling (eBDIMS) method, which is based on the Essential Dynamics-refined Elastic Network Model force field (43). Here we used the eBDIMS server with the default parameters.

### Electrostatic potential surfaces

The electrostatic potential molecular surface was calculated using the Adaptive Poisson-Boltzmann Solver (APBS) software (44). The required partial charges to molecule preparation were performed by PDB2PQR software (45). The electrostatic maps were calculated using the default parameters and the results were display using the potential at the solvent accessible surface for coloring. All procedures were done using the APBS Electrostatics Plugin into PyMOL2.0 (46).

### Quantum mechanics cluster calculations

Cluster models were constructed from the last structures of the simulations in each situation, and geometry optimized with the exchange-correlation functional B3LYP and the basis set 6–31G(d) (47). The free protein has a total of 151 atoms, whereas the complex with DFU has 173 atoms and GLU has 186 atoms. The atoms of the protein residues cleaved bonds were kept frozen during the calculations.

### Microbial strains

*Escherichia coli* strains used in this study were MG1655 with *uxuB* knockout (MBR) and MG1655(DE3) with *gudD, uxaC* and *uxuR* knockouts (M2BR) (Supplementary Table S1). Knockout strains were made from parent strains MG1655 and MG1655(DE3) with *gudD* and *uxaC* knockouts (MG1655(DE3)Δ*gudD*Δ*uxuR*), respectively, using the λ Red knockout protocol (48) to sequentially delete *uxuB* and *uxuR* from the parent strains. Removing *uxuB* prevents the consumption of DFU and removing *uxuR* prevents interference from endogenous UxuR. λ-Red-mediated recombination was done using pKD46 with primers uxuB_FWD/uxuB_REV and uxuR_FWD/uxuR_REV for *uxuB* and *uxuR* knockouts, respectively (Supplementary Table S2). These primers were used to amplify the corresponding knockout cassette (flanked by FLP recognition target sites) from the Keio collection strains (49). MG1655 and MG1655(DE3)Δ*gudD*Δ*uxuR* harboring pKD46 were transformed sequentially, first with the *uxuB* cassette (forming intermediate strains MG1655 with *uxuB* knockout (MB) and MG1655 with *gudD, uxaC* and *uxuB* knockouts (M2B), intermediate strains and then with the *uxuR* cassette. Following transformation, the *kan* selection cassette was cured of successful deletion mutants using FLP recombinase expressed from pCP20, generating strains MBR and M2BR.

### Sensor plasmid construction

All primers used in this study are listed in Supplementary Table S2. All plasmids used in this study are listed in Supplementary Table S3. Also, a diagram depicting the biosensor plasmid is available in the Supporting Information (Supplementary Figure S1).

The biosensor plasmid was generated from plasmid pSNR1. Briefly, pSNR1 is a modified form of pHHD01K (50) that contains a p15A origin of replication, an *mRFP* gene from pTrc-RFP (located between EcoRI and BamHI cut sites located in pHHD01K) and a *gfp*(mut3b) gene from the Registry of Standard Biological Parts, part BBa_E0040 (http://www.partsregistry.org). *mRFP* is under control of the pTet promoter with RBS sequence TCACACAGGAAAG and an rrnB terminator B0010. *Gfp*(mut3b) is under control of a *cpk* promoter (see Supplementary Table S4 for sequence), with RBS sequence TA TAGGGAG, and a B0014 terminator. The TetR cassette from pHHD01K was modified with a B1002 terminator. All terminators and the *mRFP* RBS sequence (Bba_0032) are from the Registry of Standard Biological Parts (http://www.partsregistry.org).

A negative control plasmid containing no *gfp*, pSNR1MCS, was generated from pSNR1 by replacing the *gfp* gene with a multiple cloning site. The multiple cloning site was generated by an oligo anneal of primers pSNR1 MCS FWD and pSNR1 MCS REV. The annealed oligo and pSNR1 were both digested with SacI and NotI and ligated together to form pSNR1MCS.

To incorporate a hybrid promoter for *gfp* that contained a UxuR binding site, the full-length hybrid promoter sequence was generated by polymerase chain reaction (PCR) amplification using primers SacI_Prom_FWD and AflII_Prom_REV that contained overlapping regions. These primers annealed to each other for amplification (with no additional template DNA required) to form the desired insert and digestion sites. The final promoter sequence generated was: TTTACAaattggtataccaatttTATTATgctagcAcgtg caatttttaaaattaaaggcgttacccaactatagggag. −35 and −10 sequences and transcription start site are capitalized, with the binding site of UxuR located between the −35 and −10 sequences (Aaattggtataccaattt). −35 and −10 sites are from promoter J23101 from the Registry of Standard Biological Parts (http://www.partsregistry.org) and the UxuR binding site is from the promoter of the *uxuR* gene from *E. coli* (20). This PCR product and the pSNR1 backbone were both digested with SacI and AflII and ligated together. This formed the preliminary vector, pSNR1U.

To enable higher levels of *gfp* translation, a modified RBS was incorporated into pSNR1U using circular polymerase extension cloning (CPEC) (51). This new hybrid promoter region, Upro, (tttacaaattggtataccaatttttattatg ctagcacgtgcaatttttaaaattaaaggcgttacccaacAGAGG AGAa atactag) contained the same promoter, J23101, but a new, stronger RBS (capitalized). pSNR1U was amplified using primers FWD_Plasmid_CPEC_pSNR1U-Upro and REV_Plasmid_CPEC_pSNR1U-Upro, and the insert was generated by PCR with primers FWD_CPEC_pSNR1U-Upro_Insert and REV_CPEC_pSNR1U-Upro_Insert that contained overlapping regions for CPEC. As before, the insert primers self-annealed, allowing amplification without the need for template DNA. The backbone and insert were annealed and amplified by CPEC to generate the final positive control plasmid, pSNR1-Upro. This resulted in a positive control plasmid that contained no *uxuR* and expressed GFP constitutively in a *uxuR* knockout strain.

To incorporate the *E. coli uxuR* gene and create pSNR1-UxuR-Upro, primers BsaI_UxuR_FWD and BsaI_UxuR_REV were used to PCR amplify *uxuR* from *E. coli* genomic DNA. The PCR product was digested with BsaI (leaving Eco-RI and SacI sticky ends) and the pSNR1-Upro backbone was digested with EcoRI and SacI. The amplified gene and digested backbone were ligated to form pSNR1-UxuR-Upro.

Mutant ConstructionSite-directed mutagenesis was performed using the Q5 Site-Directed Mutagenesis (SDM) kit (New England BioLabs, Ipswich, MA, USA). Briefly, the pSNR1-UxuR-Upro plasmid was amplified with primers MutA1-A4_F and MutA1-A4_R (Supplementary Table S3). The primers A1-A4 amplified the entire vector and contained the desired mutagenized bases for mutations H152A, H201A, H223A and D148A, respectively. The amplified PCR product was digested with Dpn1 enzyme to remove

template DNA at 37°C for 45 min and gel purified. The purified product was ligated using the SDM kit (per manufacturer instructions) and the ligation product used to transform DH5α.

Colonies were sequenced to verify the presence of the desired mutation using primers pTet_Forward and pHHD01K_Term_Rev. All restriction enzymes, ligases, and polymerases were purchased from New England Biolabs (Ipswich, MA, USA).

### Fermentation and GFP measurement

Strain MBR was transformed with the positive control of the biosensor (pSRN1-Upro), the negative control of the biosensor (pSNR1MCS), the original, unmutated biosensor (pSNR1-UxuR-Upro) and the mutated versions of the biosensor (Supplementary Table S3). Overnight cultures of transformants were grown overnight in LB with 50 μg/ml kanamycin at 37°C. Fermentation cultures were inoculated from overnight cultures in LB and 50 μg/ml kanamycin at a dilution of 1:100 vol/vol. Fermentation was carried out for 24 h in the BioLector (m2p labs, Baesweiler, Germany). Cultures were grown in FlowerPlates (m2p labs) containing 1 ml medium per well, at 37°C, 1200 rpm, 80% relative humidity. The wells contained LB or LB medium supplemented with 3 mM GLU; 50 μg/ml kanamycin was added to all cultures. Medium in which the biosensor plasmid and mutant variants were cultured was additionally supplemented with 50 ng/ml aTc for induction of *uxuR* from the pTet promoter. Biomass (backscattered light at 620 nm) and GFP (488 nm excitation/520 nm emission) measurements were taken by the BioLector every ∼15 min. GFP units as measured by the BioLector were normalized by biomass units from the BioLector for data analysis.

### Statistics

MATLAB statistics software was used to perform a right-tailed *t*-test assuming unequal variances to compare the normalized GFP signals. To compare the fold change in GFP of the unmutated biosensor to the fold change in GFP of the mutated biosensor a left-tailed *t*-test assuming unequal variances was used.

## RESULTS AND DISCUSSION

### Substrate binding to UxuR

The proteins of the GntR superfamily contain a remarkably conserved DNA-binding winged helix-turn-helix (wHTH) domain at the N-terminal region (NTD) and an effector-binding domain (EBD) at the C-terminal region (CTD) used to define GntR subfamilies. Upon binding of an effector molecule, a conformational change occurs, influencing the DNA-binding properties of the TFs, resulting in repression or activation of gene transcription (52). The nature of this mechanism is not described for any member of the GntR subfamily.

Here, we have built a new model for the aTF UxuR (Supplementary Figure S2 and S3). We have taken all the sequence information about the GntR superfamily into account. Our results show that UxuR is a dimer, which is typical for the FadR subfamily (53). The NTD of our model is formed by three α helices and three β strands. The CTD region is composed of six α helices, thus the aTF UxuR can be included in the FCD family (54). The wHTH and EBD domains are connected through a linker. Usually, this linker, composed of flexible residues, vary in secondary structure and length (from ∼ 5 to 25 amino acids) (55,56). UxuR linker model is formed by 21 amino acids, the last one being a proline residue which has been identified as a more frequent terminal linker residue, because of its rigidity that prevents unfavorable contacts between domains that could be as an unwanted result of the high flexibility of the linkers (55). The connecting between domains through a linker has an important consideration in protein architecture and function, which are both flexible and allosterically regulated (55,56). In the aTF UxuR model, we predicted some residues implied in the allosteric mechanism. The most common mode of coordination of a Zn(II) ion is via four atoms (57). The residues that dominate zinc-binding sites are well established: histidine, aspartate, glutamate and cysteine (58,59). Sequence analysis showed that most FadR TFs, namely the FadR C-terminal domain (FCD) family (Pfam-PF07729(4)), contain three conserved histidine residues and one aspartate residue, supporting the probability of metal dependence (1,13). For the UxuR model, we suggest that the conserved residues of the zinc-binding motif are composed of three histidine residues (H152, H201 and H223) and one aspartate (D148) (Figure 1). The cationic dummy atom (CaDA) method used to describe Zn(II) ion in aTF UxuR model, provides a reasonable description for Zn(II) ion's first coordination sphere (60). Our results show that during the MD simulations, the Zn(II) ion keeps its position. However, to further assess Zn(II) ion coordination we performed Quantum Mechanic (QM) cluster model calculations with the last structures of the simulations (Figure 1).

Based on the information of the closest homologs (15) and our molecular docking studies, we have identified a pocket in the CTD close to the Zn(II) ion as the most probable region for substrate binding and coordinates to the substrates. We were able to identify interactions between the ligands and the protein after performing independent MD simulations for the three situations: i) free protein, ii) bound to DFU and iii) bound to GLU. Observing the free form situation (Figure 1A), the Zn(II) ion binds to the three histidine residues (H152, H201 and H223) and D148. When the UxuR is bound to their inducer (Figure 1B) and GLU (Figure 1C), the H152 side-chain rearrange its position allowing the binding of ligands to the Zn(II) ion and maintain the coordination via four atoms. Our results are in good agreement with recent literature, the average distance of metal-ligand for nitrogen atoms is 2.12 ± 0.19 Å and for oxygen atoms is 2.31 ± 0.54 Å (57). To verify our *in silico* results, we performed site-directed mutagenesis of the histidines and the aspartate residues. As expected, the single mutations of the histidine and the aspartate residues negatively interfere with ligand binding to UxuR (more detailed results are discussed below). These results are in unanimity with our computational predictions and reveal the important role of these four residues in allosteric regulation with the ligand. Also, the structural analysis revealed that the residues

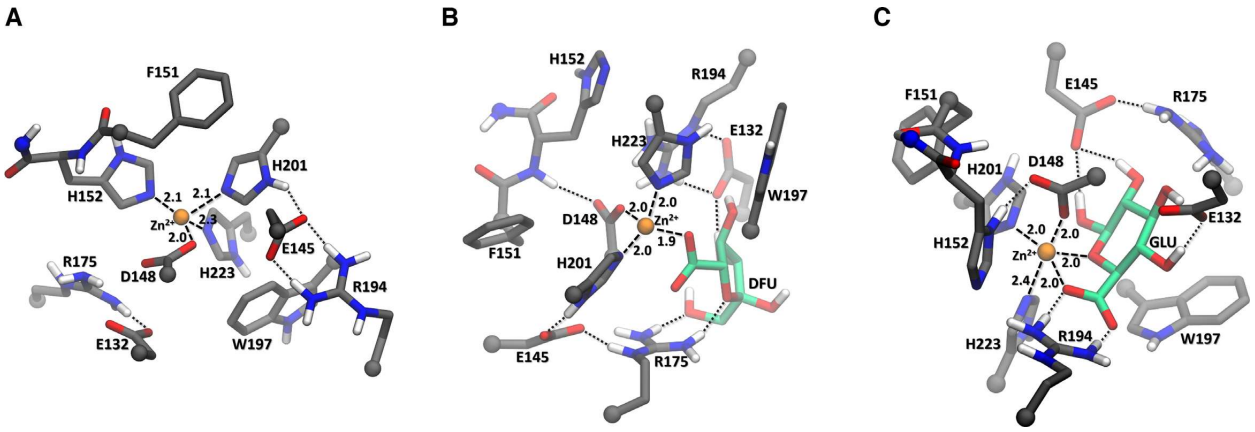


**Figure 1.** Quantum Mechanic cluster model structures from the UxuR MD simulations, showing the (**A**) free form, (**B**) DFU and the (**C**) GLU carboxylate oxygen atoms binding to the Zn(II) ion (sphere colored orange).

were in the correct orientation to coordinate to Zn(II) ion.

### Substrate binding affects the dynamical behavior of the protein

Having determined the binding site for the substrates, we then studied the dynamic behavior of the protein for the three situations. When the ligands are bound, local changes generate an allosteric response, leading to a conformational change of UxuR. At this moment, the stimulus resulting from the perturbation caused by the ligand binding it is propagated by the linkers, from the EBD to the NTD. The flexibility of linkers allows the propagation of a signal that results in different conformational changes. The after-effect is the fast reorientation of one domain (CTD) to another (NTD). The barriers implicate in these conformational changes are quite low. Thus, molecular movements can be observed and analyzed during nanosecond simulations (56,61–63). In our study, the Root-Mean-Square Deviations (RMSDs) and Root-Mean-Square Fluctuations (RMSFs) by residue, are provided for each simulation in the SI. As it is possible to observe in Supplementary Figure S4, the values are large for all structures, showing that the structures are quite flexible and that significant domain movement occurs during our simulations. To dissect the nature of such movements, we performed PCA to extract the dominant modes in the UxuR motion from the MD simulations. By calculating the eigenvectors from the covariance matrix of a simulation we have identified the dominant motions. Briefly, the Principal Component (PC) is a vector describing the relative contribution of each selected atom's x, y and z component to the correlated mode of motion corresponding to that component (64). Here, we show for different approaches the differences between the motions in the free protein and the protein bound with either ligand. On the 2D plane projections (Figure 2 and Supplementary Figures S5–S7), each simulation frame onto a given PC is the dot product of the alpha carbon (Cα) coordinates of that frame with the PC vector. In general, for the free form situation and the one bound to DFU, the three largest PCs (PC1, PC2 and PC3) account for more than 70% of the motions (Supplementary Figures S5 and S6). However, the GLU bound situation seems to be characterized by a more complex movement, since the three first PCs were not enough to identify the dominant motions (Supplementary Figure S7). At the free protein, the two NTDs (which bind the DNA) are close together (in what we will call from now on a closed conformation) and vibrate around this position in a parallel orientation and opposite directions (Figures 2A and B; Supplementary Figure S8). When DFU binds to UxuR at the CTD region, the movements of the NTD regions are counterclockwise or clockwise twists, with a more pronounced movement of one chain (Figures 2C and D; Supplementary Figure S9). On the other hand, when GLU binds to UxuR, the movements of the NTD regions are closure twists (Figures 2E and F; Supplementary Figure S10). This movement with the GLU ligand seems to allow for the approximation of the NTD regions and the binding to the DNA. Based on results from the first two PCs, we constructed and analysed the FEL of the systems understudy (free form, bound to DFU and GLU) at 300 K (Figure 3). Our results show different minima denoting the stable states (darkest colored) and the associated higher-energy transient states (light colors) (Figure 3A, C and E). The free form FEL is significantly different from the bound systems, with just one minimum during the simulation time (Figure 3A and B). The bound-states display a lower-energy minimum and other smaller minima (Figure 3C–F). The DFU form has the largest global minimum and this is in a different position when compared to the other situations. Our results are in accordance with previous data that points to dynamic ensembles of a swiftly conformational switch, which can be described by relatively flat energy landscapes (65). For example, the ZitR TF, which contains a linker connecting two domains, displays conformational changes that amount to free energy barriers around 3 kcal/mol (63). In our work, the conformational changes observed through the simulations for the three systems are also characterized by low free energy barriers of about 3.2 kcal/mol.

Comparing the global minimum structures from the PCA and FEL analysis (Supplementary Figure S11), we can observe more identical conformations between the free form and the one bound to GLU (Supplementary Figure S11a),

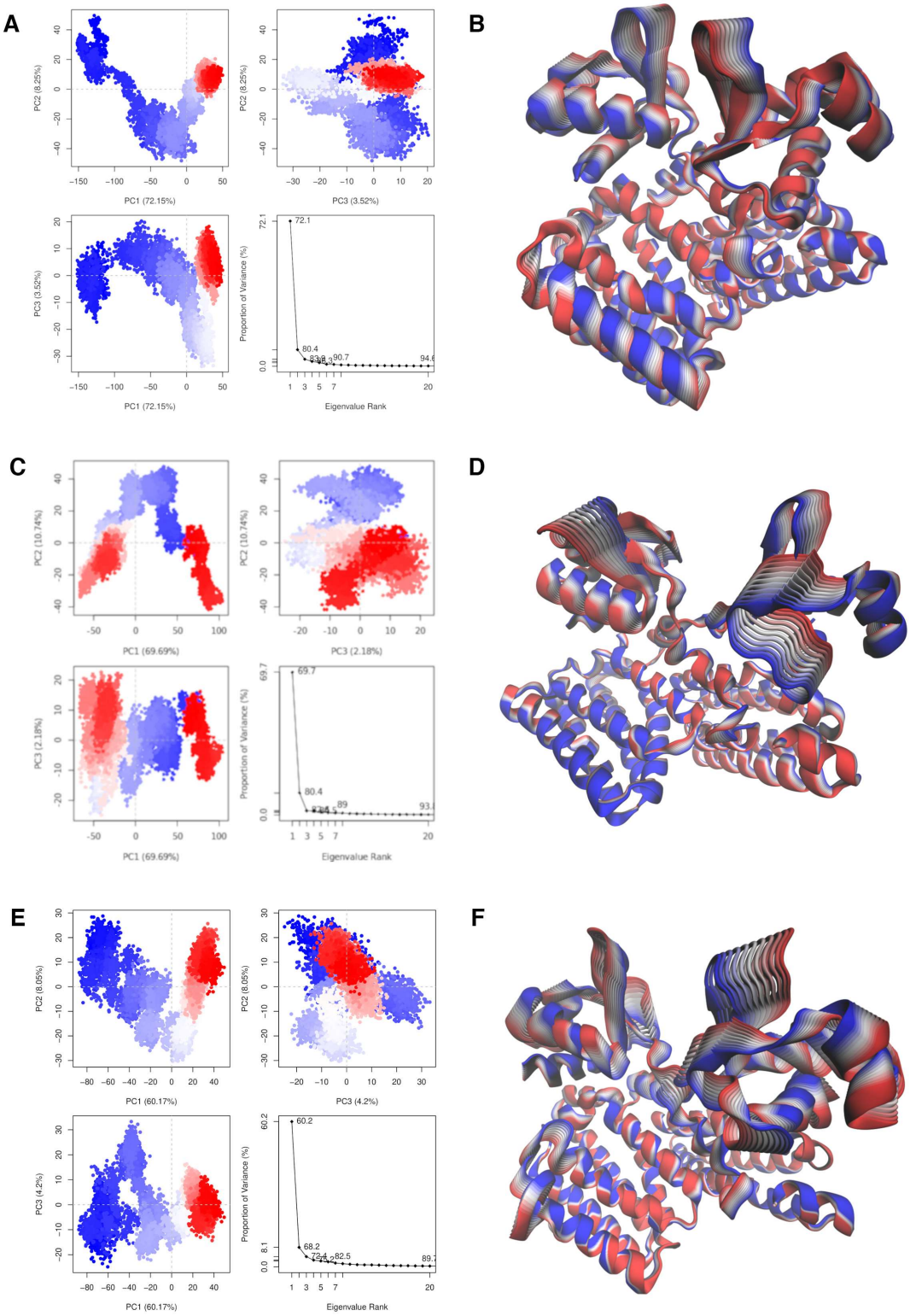


**Figure 2.** Right: Bio3D plot of PCA results for trajectory frames colored from blue to white to red in order of time. Left: The structures are shown as a backbone trace at the front view. The colors summarize the direction of motion, from blue to white to red. (**A**) and (**B**) UxuR free form; (**C**) and (**D**) UxuR bound to DFU; (**E**) and (**F**) UxuR bound to GLU.

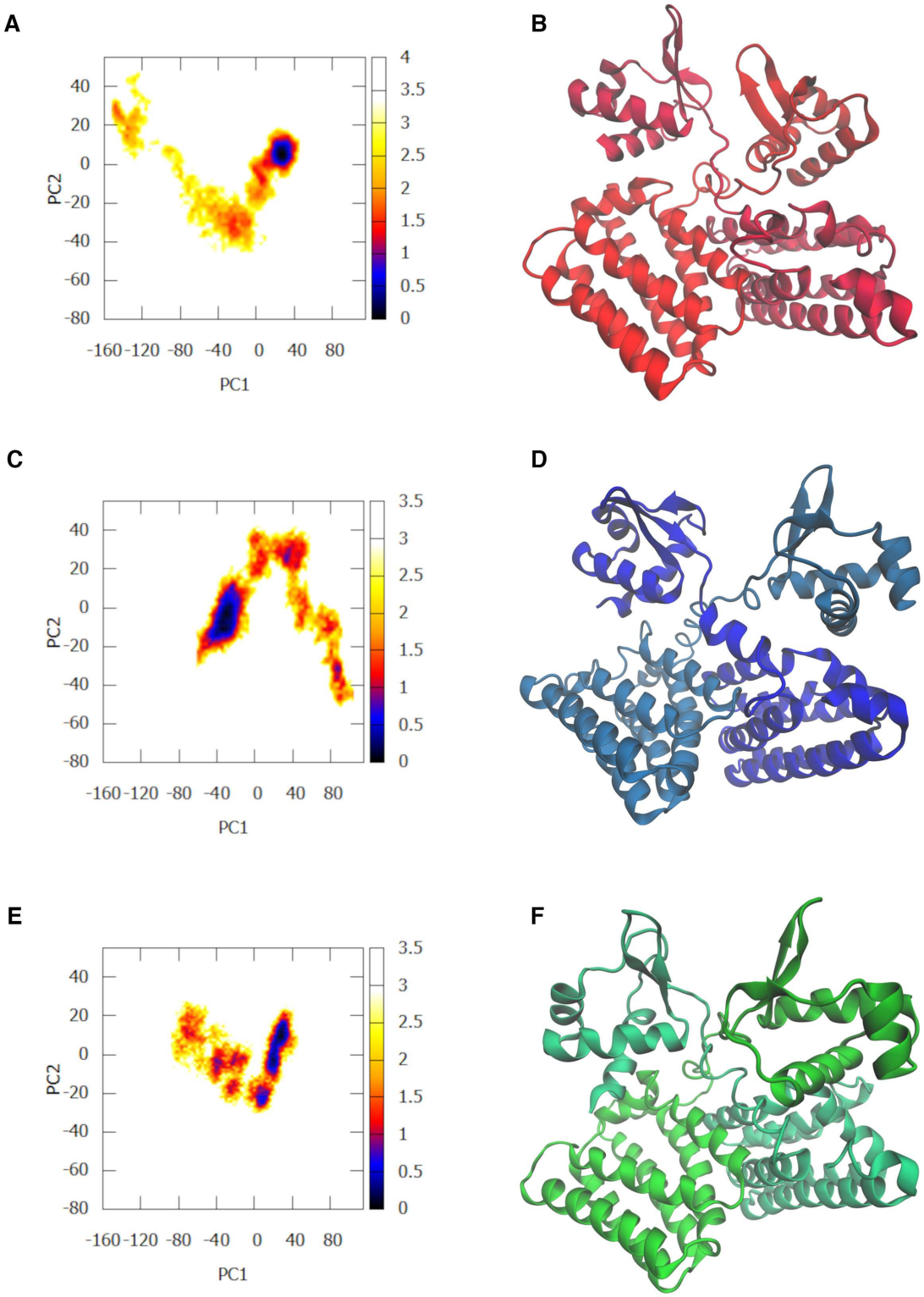


**Figure 3.** Two-dimensional FEL (in kcal/mol) of PC1 and PC2 of the free form protein (**A** and **B**) and protein ligand complex (**C** and **D**: DFU; **E** and **F**: GLU) at 300 K. Deeper color areas in the maps indicate lower energy. The global minima structures are shown as a backbone trace at the front view: red—free from, blue—bound to DFU and green—bound to GLU.

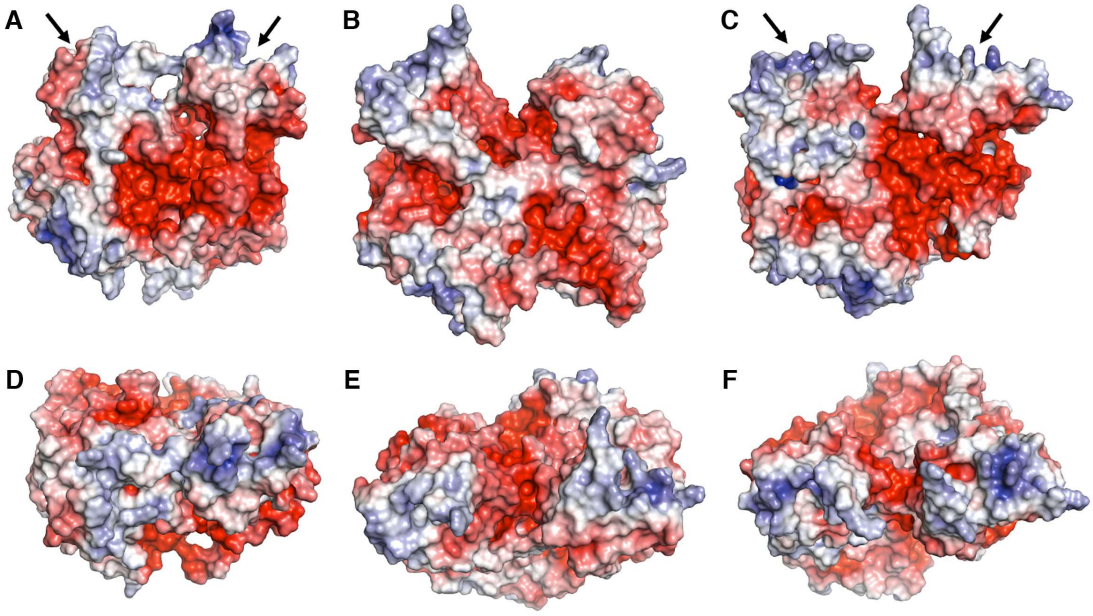


**Figure 4.** Electrostatic surface of UxuR: (**A** and **B**)—free form; (**C** and **D**)—UxuR bound to DFU; (**E** and **F**)—UxuR bound to GLU. The surface structures are shown at the front (A, C and E) and top views (B, D and F). The blue color indicates regions of positive potential whereas red shows negative potential values. The black arrows indicate the more probable DNA-binding sites.

than with the DFU form (Supplementary Figure S11b). These results are in good agreement with the dominant motions observed during the simulations. Contrary to what happens when the DFU is present, binding of the GLU still favors the bound conformation, which may explain the ability of UxuR to remain bound to DNA, as it happens in the free form.

For more detailed quantitative results of the motions in aTF UxuR model, we used the eBDIMS server (66). The eBDIMS selects the major normal modes (NMs) of the start structure for projection, i.e. the two NMs better overlapped with the modeled transition, representing more than 80% of the movements involved. Analyzing the DFU and GLU situations (Supplementary Figure S12), we observe a similar molecular movement denoting the allosteric conformational alteration. On the other hand, the free situation is distinct, which is in good agreement with the data resulting from the PCA and FEL. These results support the difference of motions between the three situations that indicated whether or not the aTF UxuR is bound to the DNA.

Based on our results during all simulations (Figures 2, 3 and Supplementary Figure S5–S12), we can establish a movement pattern for each situation, and we hypothesize that the closing movement of the chains allows the protein to bind to the DNA. This is in accordance with the flexibility of the linkers. The binding of the ligands causes a perturbation through the linkers that leads to a conformational change and reorientation of protein inter-domains region (56). Here, this allosteric propagation force seems to have different behavior whether DFU or GLU are bound to the protein.

To better understand how the allosteric regulation compromises the conformational behavior of the UxuR, we analyze the alteration of the residues side-chain on the NTD. The electrostatic surface calculations for UxuR in free and bound forms show differences at the NTD region that can further explain the binding to the DNA (Figure 4). In the free protein, the two NTD regions remain close, leading to a continuous stretch of positively charged residues in the region that binds the DNA (Figure 4A). In the structure with DFU, the two N-termini are farther apart and the negatively charged interface is more visible. This change in the protein surface charge can adversely impact binding to the DNA (which is also negatively charged) (Figure 4B). In the structure with GLU, the NTD regions are still connected, but instead of being in a parallel orientation, they are diagonally oriented (Figure 4C). It should be noted that these changes are dynamic; the NTD in the free protein remain to oscillate between closed conformations, whereas in the protein with GLU bound we observe a switch between open and closed conformations. If we consider only the crystal structure of FADR (PDB code: 1H9T) with bound DNA, we can observe that the two NTDs are in a closed conformation binding side-by-side to the major groove and different minor-groove regions (Supplementary Figure S13). Similarly, our free-protein and the protein–GLU complex can adopt closed conformations (albeit different ones), while the protein–DFU complex can sample an open-conformation. Furthermore, the movement promoted by DFU binding seems to be incompatible with closed conformations. More information about the electrostatic surface of UxuR can be found in the Supplementary Figures S14–S16.

### Validation of the fructuronic acid biosensor

To allow for experimental observation of the importance of the aspartate and histidine residues upon UxuR function, a

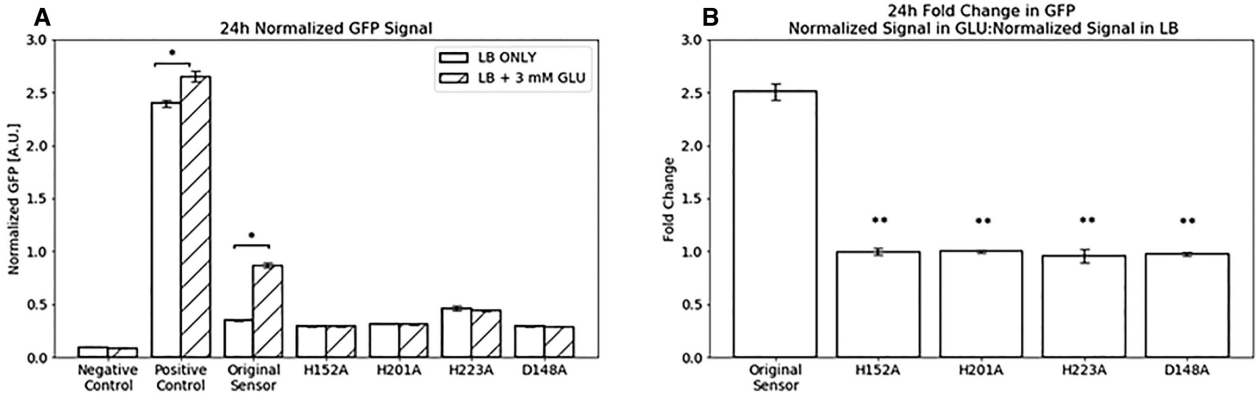


**Figure 5.** (**A**) Normalized GFP for each sample at 24h. * indicates a normalized GFP signal in GLU supplemented media that is significantly ($P < 0.05$) higher than normalized GFP signal in unsupplemented media). (**B**) Fold change in normalized GFP in the presence of GLU. ** indicates a fold change in GFP that is significantly ($P < 0.05$) lower than observed in the biosensor. Error bars represent ±1 SD from the mean of three replicate cultures.

TF based biosensor that responds to DFU was successfully constructed and validated. This biosensor contained a regulator, *uxuR* and a fluorescent reporter, *gfp*. The positive and negative control set upper and lower bounds, respectively, on the expected normalized GFP signal (Figure 5A).

The UxuR operator site was located within a hybrid promoter upstream of the reporter gene. Upon expression of UxuR from the biosensor plasmid, pSNR1-UxuR-Upro, *gfp* transcription was repressed. This repression was alleviated upon allosteric binding by the ligand, DFU and resulting GFP levels correlated to the amount of ligand present. The ability of DFU to allosterically bind to the UxuR binding site and relieve transcriptional repression has been shown previously (19).

DFU is not commercially available; however, its structural isomer, GLU, is. DFU is formed through the isomerization of GLU via uronate isomerase (UxaC) (67). GLU can serve as a carbon source for *E. coli* (68) but cannot be metabolized in the absence of UxaC (69). UxaC can thus serve to convert GLU to DFU (which is then further metabolized through D-mannonate reductase, UxuB). We exploited this catabolic pathway to produce DFU *in situ* from GLU. Experiments were conducted in strain MBR, with knockouts of *uxuB* and genomic *uxuR*.

The expected biosensor behavior was observed as the GFP signal was found to be significantly higher in the presence of DFU (Figure 5B). The biosensor was not functional in a *uxaC* knockout strain (M2BR) confirming that the biosensor responds to DFU and not GLU (Supplementary Figure S17).

Further, the response of the biosensor to DFU (via 3 mM GLU) showed a clear switching dynamic with a slight lag (~2 h) in biosensor response that is possibly due to the isomerization of GFU to DFU (Supplementary Figure S18). The dynamics of this response are similar to the responses shown in the successful application of sensor-regulation for pathway control (70,71). This indicates a potential for further application of the UxuR biosensor as a regulatory element.

This experiment was run with both positive (pSNR1-Upro) and negative (pSNR1MCS) control plasmids. The positive control plasmid had the same hybrid promoter and GFP gene as the sensor, but had no *uxuR* present on the plasmid, allowing for constitutive expression of GFP. The negative control contained the same *uxuR* gene as the biosensor but was lacking the *gfp* gene.

### Mutations in the zinc coordination sphere

Mutations H152A, H201A, H223A and D148A were designed to disrupt the coordination of zinc-binding. Thus, testing the response of these mutants with the biosensor should reveal whether ligand binding is also disrupted. The *uxuR* mutants were incorporated in the biosensor plasmid, and the response to DFU was evaluated in MBR strains containing biosensor variants. In the mutant variants, no de-repression was observed upon the addition of GLU to the media (Figure 5B). The fold change in GFP response observed by the unmutated biosensor is significantly higher than all UxuR mutants suggesting that only the original biosensor retained the ability to respond to DFU while the mutants did not. Of note is the observation that there was a slight increase in the basal (leaky) biosensor signal from mutant H223A. This suggests that this particular mutation may have also impacted the affinity of UxuR for its cognate binding site within the promoter.

## CONCLUSION

The GntR superfamily, broadly distributed throughout the bacteria and known to regulate essential biological processes, gives an appealing opening in the development of inducible and controllable expression systems. The presence of metals in the GntR superfamily was reported for the first time in the repressor LldR from *Corynebacterium glutamicum* (PDB code: 2DI3) involved in L-lactate and fructose/glucose utilization (15). Recently, Kotowska *et al.* described a Zn(II) ion binding a protein named HypR and suggested that zinc is a co-factor involved in the binding of an organic compound. Yet, the mechanism is still not clear (12). Zheng *et al.* solved the crystal structure of *Thermotoga maritima* TM0493—UxaR (PDB code: 3FMS), a regulator with a Zn(II) ion binding the effector domain involved in the regulation of hexuronic acid metabolism (13,72,73). The

physiological role of the Zn(II) ion and its interaction was not described. Blancato *et al*. showed that in CitO, a regulator of citrate metabolism from *Enterococcus faecalis*, the coordination of a metal ion is crucial for binding of the citrate molecule and effective DNA binding (14). As we previously referred, it has been unclear if these GntR TFs are metal sensing or if the metal plays a structural role or is required for binding of other effector molecules (12,13,15). Thus, an understanding of the molecular mechanisms of regulation is required.

In this work, we have built a new homology model for the TF UxuR and performed docking and MD simulations. Our results show that this protein contains the conserved motif of three histidine residues and aspartate in a correct position to coordinate one Zn(II) ion. Furthermore, we showed that the substrate binds at the CTD and coordinates to the Zn(II) ion. We identified different fast motions of the protein that are dependent on the presence and identity of the bound substrate (i.e. there is no bound substrate, D-glucuronate or D-fructuronate). The different motions led to changes at the N-terminal positively charged surface that binds to the DNA. In both the unbound TF and the TF bound to GLU, the protein samples closed conformations that promote DNA binding; however, DFU binding to Zn(II) ion drives a change in UxuR domain movements, allowing the protein to sample an open conformation. We validated our predictions by showing that the mutations predicted to disrupt the zinc-binding motif led to an inability of the mutants to respond to fructuronic acid.

Here we propose and experimentally confirm, for the first time that the Zn(II) ion fills a role in the UxuR TF allosteric mechanism by modulating DNA binding. We further explain how this can be achieved by showing large differences in the NTDs between the different complexes.

## SUPPLEMENTARY DATA

Supplementary Data are available at NARGAB Online.

## ACKNOWLEDGEMENTS

The authors acknowledge the Coimbra Institute of Engineering (ISEC) through the Minerva HPC and the National Distributed Computing Infrastructure (INCD) funded by FCT and FEDER under the project 01/SAICT/2016 nº 022153 for computational resources and also the projects CPCA/A2/4568/2020 and CPCA/A2/4595/2020.
*Author Contributions*: The manuscript was written through the contributions of all authors. All authors have approved the final version of the manuscript.

## FUNDING

This work was financed by Portuguese national funds via FCT - Fundação para a Ciência e a Tecnologia, under Projects MIT-Portugal seed project 6937814, UIDB/04539/2020, Grants IF/01272/2015, SFRH/BD/144303/2019 and SFRH/BD/150697/2020, and through the COMPETE 2020 - Operational Programme for Competitiveness and Internationalisation.
*Conflict of interest statement.* None declared.

## REFERENCES

1. Jain,D. (2015) Allosteric control of transcription in GntR family of transcription regulators: A structural overview. *IUBMB Life*, **67**, 556–563.
2. Beckett,D. (2009) Regulating transcription regulators via allostery and flexibility. *Proc. Natl Acad. Sci. U.S.A.*, **106**, 22035–22036.
3. Taylor,N.D., Garruss,A.S., Moretti,R., Chan,S., Arbing,M.A., Cascio,D., Rogers,J.K., Isaacs,F.J., Kosuri,S., Baker,D. *et al.* (2016) Engineering an allosteric transcription factor to respond to new ligands. *Nat. Methods*, **13**, 177–183.
4. El-Gebali,S., Mistry,J., Bateman,A., Eddy,S.R., Luciani,A., Potter,S.C., Qureshi,M., Richardson,L.J., Salazar,G.A., Smart,A. *et al.* (2019) The Pfam protein families database in 2019. *Nucleic Acids Res.*, **47**, D427–D432.
5. Rigali,S., Derouaux,A., Giannotta,F. and Dusart,J. (2002) Subdivision of the helix-turn-helix GntR family of bacterial regulators in the FadR, HutC, MocR, and YtrA subfamilies. *J. Biol. Chem.*, **277**, 12507–12515.
6. Jaques,S. and McCarter,L.L. (2006) Three new regulators of swarming in *Vibrio parahaemolyticus*. *J. Bacteriol.*, **188**, 2625–2635.
7. Hoskisson,P.A., Rigali,S., Fowler,K., Findlay,K.C. and Buttner,M.J. (2006) DevA, a GntR-like transcriptional regulator required for development in *Streptomyces coelicolor*. *J. Bacteriol.*, **188**, 5014–5023.
8. Ostash,B., Rebets,Y., Myronovskyy,M., Tsypik,O., Ostash,I., Kulachkovskyy,O., Datsyuk,Y., Nakamura,T., Walker,S. and Fedorenko,V. (2011) Identification and characterization of the *Streptomyces globisporus* 1912 regulatory gene lndYR that affects sporulation and antibiotic production. *Microbiology (Reading, Engl.)*, **157**, 1240–1249.
9. Truong-Bolduc,Q.C. and Hooper,D.C. (2007) The transcriptional regulators NorG and MgrA modulate resistance to both quinolones and beta-lactams in *Staphylococcus aureus*. *J. Bacteriol.*, **189**, 2996–3005.
10. Reuther,J., Wohlleben,W. and Muth,G. (2006) Modular architecture of the conjugative plasmid pSVH1 from *Streptomyces venezuelae*. *Plasmid*, **55**, 201–209.
11. Casali,N., White,A.M. and Riley,L.W. (2006) Regulation of the *Mycobacterium tuberculosis* mce1 operon. *J. Bacteriol.*, **188**, 441–449.
12. Kotowska,M., Świat,M., Zaręba-Pasławska,J., Jaworski,P. and Pawlik,K. (2019) A GntR-like transcription factor HypR regulates expression of genes associated with L-Hydroxyproline utilization in *Streptomyces coelicolor* A3(2). *Front. Microbiol.*, **10**, 1451.
13. Zheng,M., Cooper,D.R., Grossoehme,N.E., Yu,M., Hung,L.-W., Cieslik,M., Derewenda,U., Lesley,S.A., Wilson,I.A., Giedroc,D.P. *et al.* (2009) Structure of *Thermotoga maritima* TM0439: implications for the mechanism of bacterial GntR transcription regulators with $Zn^{2+}$-binding FCD domains. *Acta Crystallogr.*, **65**, 356–365.
14. Blancato,V.S., Pagliai,F.A., Magni,C., Gonzalez,C.F. and Lorca,G.L. (2016) Functional analysis of the citrate activator CitO from *Enterococcus faecalis* implicates a divalent metal in ligand binding. *Front. Microbiol.*, **7**, 101.
15. Gao,Y.G., Suzuki,H., Itou,H., Zhou,Y., Tanaka,Y., Wachi,M., Watanabe,N., Tanaka,I. and Yao,M. (2008) Structural and functional characterization of the LldR from Corynebacterium glutamicum: a transcriptional repressor involved in l-lactate and sugar utilization. *Nucleic Acids Res.*, **36**, 7110–7123.
16. Bouvier,J.T., Sernova,N.V., Ghasempur,S., Rodionova,I.A., Vetting,M.W., Al-Obaidi,N.F., Almo,S.C., Gerlt,J.A. and Rodionov,D.A. (2018) Novel metabolic pathways and regulons for hexuronate utilization in proteobacteria. *Bacteriol*, **201**, e00431-18.
17. Ritzenthaler,P., Mata-Gilsinger,M. and Stoeber,F. (1980) Construction and expression of hybrid plasmids containing *Escherichia coli* K-12 uxu genes. *J. Bacteriol*, **143**, 1116–1126.
18. Rodionov,D.A., Mironov,A.A., Rakhmaninova,A.B. and Gelfand,M.S. (2000) Transcriptional regulation of transport and utilization systems for hexuronides, hexuronates and hexonates in gamma purple bacteria. *Mol. Microb.*, **38**, 673–683.
19. Bates Utz,C., Nguyen,A.B., Smalley,D.J., Anderson,A.B. and Conway,T. (2004) GntP Is the *Escherichia coli* fructuronic acid transporter and belongs to the UxuR regulon. *J. Bacteriol.*, **186**, 7690–7696.
20. Tutukina,M.N., Potapova,A.V., Vlasov,P.K., Purtov,Y.A. and Ozoline,O.N. (2016) Structural modeling of the ExuR and UxuR

transcription factors of *E. coli*: search for the ligands affecting their regulatory properties. *J. Biomol. Struct. Dyn.*, **34**, 2296–2304.
21. Purtov,Y.A., Tutukina,M.N., Nikulin,A.D. and Ozoline,O.N. (2019) The topology of the contacts of potential ligands for the uxur transcription factor of *escherichia coli* as revealed by flexible molecular docking. *Biophysics*, **64**, 49–56.
22. Kim,D.E., Chivian,D. and Baker,D. (2004) Protein structure prediction and analysis using the Robetta server. *Nucleic Acids Res.*, **32**, W526–W531.
23. Little,M.S., Pellock,S.J., Walton,W.G., Tripathy,A. and Redinbo,M.R. (2018) Structural basis for the regulation of β-glucuronidase expression by human gut Enterobacteriaceae. *Proc. Natl Acad. Sci. U.S.A.*, **115**, E152–E161.
24. Pang,Y.P., Xu,K., Yazal,J.E. and Prendergas,F.G. (2000) Successful molecular dynamics simulation of the zinc-bound farnesyltransferase using the cationic dummy atom approach. *Protein Sci.*, **9**, 1857–1865.
25. Pang,Y.P. (2001) Successful molecular dynamics simulation of two zinc complexes bridged by a hydroxide in phosphotriesterase using the cationic dummy atom method. *Proteins*, **45**, 183–189.
26. Pettersen,E.F., Goddard,T.D., Huang,C.C., Couch,G.S., Greenblatt,D.M., Meng,E.C. and Ferrin,T.E. (2004) UCSF chimera—a visualization system for exploratory research and analysis. *J. Comput. Chem.*, **25**, 1605–1612.
27. Kirschner,K.N., Yongye,A.B., Tschampel,S.M., González-Outeiriño,J., Daniels,C.R., Foley,B.L. and Woods,R.J. (2008) GLYCAM06: a generalizable biomolecular force field carbohydrates. *J. Comput. Chem.*, **29**, 622–655.
28. Bayly,C.I., Cieplak,P., Cornell,W. and Kollman,P.A. (1993) A well-behaved electrostatic potential based method using charge restraints for deriving atomic charges: the RESP model. *J. Phys. Chem.*, **97**, 10269–10280.
29. Morris,G.M., Huey,R., Lindstrom,W., Sanner,M.F., Belew,R.K., Goodsell,D.S. and Olson,A.J. (2009) AutoDock4 and AutoDockTools4: automated docking with selective receptor flexibility. *J Comput. Chem.*, **30**, 2785–2791.
30. Morris,G.M., Goodsell,D.S., Halliday,R.S., Huey,R., Hart,W.E., Belew,R.K. and Olson,A.J. (1998) Automated docking using a Lamarckian genetic algorithm and an empirical binding free energy function. *J. Compt. Chem.*, **19**, 1639–1662.
31. Carvalho,A.T.P., Barrozo,A., Doron,D., Kilshtain,A.V., Major,D.T. and Kamerlin,S.C.L. (2014) Challenges in computational studies of enzyme structure, function and dynamics. *J. Mol. Graph. Model.*, **54**, 62–79.
32. Carvalho,A.T.P., Fernandes,P.A. and Ramos,M.J. (2007) The excision mechanism in reverse transcriptase: pyrophosphate leaving and fingers opening are uncoupled events with the analogues AZT and d4T. *J. Phys. Chem. B*, **111**, 12032–12039.
33. Gomes,A.S., Ramos,H., Gomes,S., Loureiro,J.B., Soares,J., Barcherini,V., Monti,P., Fronza,G., Oliveira,C., Domingues,L. *et al.* (2020) SLMP53-1 interacts with wild-type and mutant p53 DNA-binding domain and reactivates multiple hotspot mutations. *Biochim. Biophys. Acta Gen. Subj.*, **1864**, 129440.
34. Salomon-Ferrer,R., Case,D.A. and Walker,R.C. (2013) An overview of the Amber biomolecular simulation package: Amber biomolecular simulation package. *Wiley Interdiscip. Rev. Comput. Mol. Sci.*, **3**, 198–210.
35. Hornak,V., Abel,R., Okur,A., Strockbine,B., Roitberg,A. and Simmerling,C. (2006) Comparison of multiple Amber force fields and development of improved protein backbone parameters. *Proteins*, **65**, 712–725.
36. Pastor,R.W. (1994) Techniques and applications of langevin dynamics simulations. In: Luckhurst,G.R. and Veracini,C.A. (eds). *The Molecular Dynamics of Liquid Crystals*. Springer, Dordrecht, pp. 85–138.
37. Hauptman,H.A. (1997) Shake-and-bake: an algorithm for automatic solution ab initio of crystal structures. In: Carter,C.W. Jr. and Sweet,R.M. (eds). *Methods in Enzymology*. Academic Press, Cambridge, Massachusetts, Vol. **277**, pp. 3–13.
38. Darden,T., York,D. and Pedersen,L. (1998) Particle mesh Ewald: an N·log(N) method for Ewald sums in large systems. *J. Chem. Phys.*, **98**, 10089–10092.
39. Roe,D.R. and Cheatham,T.E. (2013) PTRAJ and CPPTRAJ: software for processing and analysis of molecular dynamics trajectory data. *J. Chem. Theory Comput.*, **9**, 3084–3095.
40. Grant,B.J., Rodrigues,A.P.C., ElSawy,K.M., McCammon,J.A. and Caves,L.S.D. (2006) Bio3d: an R package for the comparative analysis of protein structures. *Bioinformatics*, **22**, 2695–2696.
41. R Core Team (2020) *R: A Language and Environment for Statistical Computing*. R Foundation for Statistical Computing, Vienna.
42. Maisuradze,G.G., Liwo,A. and Scheraga,H.A. (2010) Relation between free energy landscapes of proteins and dynamics. *J. Chem. Theory Comput.*, **6**, 583–595.
43. Orellana,L., Rueda,M., Ferrer-Costa,C., Lopez-Blanco,J.R., Chacón,P. and Orozco,M. (2010) Approaching elastic network models to molecular dynamics flexibility. *J. Chem. Theory Comput.*, **6**, 2910–2923.
44. Jurrus,E., Engel,D., Star,K., Monson,K., Brandi,J., Felberg,L.E., Brookes,D.H., Wilson,L., Chen,J., Liles,K. *et al.* (2018) Improvements to the APBS biomolecular solvation software suite. *Protein Sci.*, **27**, 112–128.
45. Dolinsky,T.J., Czodrowski,P., Li,H., Nielsen,J.E., Jensen,J.H., Klebe,G. and Baker,N.A. (2007) PDB2PQR: expanding and upgrading automated preparation of biomolecular structures for molecular simulations. *Nucleic Acids Res.*, **35**, W522–W525.
46. Schrödinger,L. (2017) *The PyMOL Molecular Graphics System Schrödinger*. https://pymol.org/2/support.html.
47. Ashvar,C.S., Devlin,F.J., Bak,K.L., Taylor,P.R. and Stephens,P.J. (1996) Ab initio calculation of vibrational absorption and circular dichroism spectra: 6, 8-Dioxabicyclo[3.2.1]octane. *J. Phys. Chem.*, **100**, 9262–9270.
48. Datsenko,K.A. and Wanner,B.L. (2000) One-step inactivation of chromosomal genes in *Escherichia coli* K-12 using PCR products. *Proc. Natl Acad. Sci. U.S.A.*, **97**, 6640–6645.
49. Baba,T., Ara,T., Hasegawa,M., Takai,Y., Okumura,Y., Baba,M., Datsenko,K.A., Tomita,M., Wanner,B.L. and Mori,H. (2006) Construction of *Escherichia coli* K-12 in-frame, single-gene knockout mutants: the Keio collection. *Mol. Syst. Biol.*, **2**, 2006.0008.
50. Dhamankar,H., Tarasova,Y., Martin,C.H. and Prather,K.L.J. (2014) Engineering E. coli for the biosynthesis of 3-hydroxy-γ-butyrolactone (3HBL) and 3, 4-dihydroxybutyric acid (3, 4-DHBA) as value-added chemicals from glucose as a sole carbon source. *Metab. Eng.*, **25**, 72–81.
51. Quan,J. and Tian,J. (2011) Circular polymerase extension cloning for high-throughput cloning of complex and combinatorial DNA libraries. *Nat. Protoc.*, **6**, 242–251.
52. Hoskisson,P.A. and Rigali,S. (2009) Variation in form and function: the helix-turn-helix regulators of the GntR superfamily. In: Laskin,A.I., Sariaslani,S. and Gadd,G.M. (eds). *Advances in Applied Microbiology*. Academic Press, Vol. **69**, pp. 1–22.
53. Xu,Y., Heath,R.J., Li,Z., Rock,C.O. and White,S.W. (2001) The FadR·DNA complex transcriptional control of fatty acid metabolism in *Escherichia coli*. *J. Biol. Chem.*, **276**, 17373–17379.
54. van Aalten,D.M.F., DiRusso,C.C., Knudsen,J. and Wierenga,R.K. (2000) Crystal structure of FadR, a fatty acid-responsive transcription factor with a novel acyl coenzyme A-binding fold. *EMBO J.*, **19**, 5167–5177.
55. Wriggers,W., Chakravarty,S. and Jennings,P.A. (2005) Control of protein functional dynamics by peptide linkers. *Biopolymers*, **80**, 736–746.
56. Ma,B., Tsai,C.-J., Haliloğlu,T. and Nussinov,R. (2011) Dynamic allostery: linkers are not merely flexible. *Structure*, **19**, 907–917.
57. Ireland,S.M. and Martin,A.C.R. (2019) ZincBind—the database of zinc binding sites. *Database*, **2019**, doi:10.1093/database/baz006.
58. Auld,D.S. (2001) Zinc coordination sphere in biochemical zinc sites. In: Maret,W. (ed). *Zinc Biochemistry, Physiology, and Homeostasis: Recent Insights and Current Trends*. Springer, Dordrecht, pp. 85–127.
59. Andreini,C. and Bertini,I. (2012) A bioinformatics view of zinc enzymes. *J. Inorg. Biochem.*, **111**, 150–156.
60. Oelschlaeger,P., Schmid,R.D. and Pleiss,J. (2003) Insight into the mechanism of the IMP-1 metallo-β-lactamase by molecular dynamics simulations. *Protein Eng. Des. Sel.*, **16**, 341–350.
61. Stadler,A.M., Stingaciu,L., Radulescu,A., Holderer,O., Monkenbusch,M., Biehl,R. and Richter,D. (2014) Internal nanosecond dynamics in the intrinsically disordered myelin basic protein. *J. Am. Chem. Soc.*, **19**, 6987–6994.
62. Capdevila,D.A., Huerta,F., Edmonds,K.A., Le,M.T., Wu,H. and Giedroc,D.P. (2018) Tuning site-specific dynamics to drive allosteric activation in a pneumococcal zinc uptake regulator. *eLife*, **7**, e37268.

63. He,X., Ni,D., Zhang,H., Li,X., Zhang,J., Fu,Q., Liu,Y. and Lu,S. (2020) Zinc-mediated conformational preselection mechanism in the allosteric control of DNA binding to the zinc transcriptional regulator (ZitR). *Sci. Rep.*, **10**, 13276.
64. Pearson,K.F.R.S. (1901) LIII. On lines and planes of closest fit to systems of points in space. *Lond. Edinburgh Dublin Philos. Magaz. J. Sci.*, **2**, 559–572.
65. van der Lee,R., Buljan,M., Lang,B., Weatheritt,R.J., Daughdrill,G.W., Dunker,A.K., Fuxreiter,M., Gough,J., Gsponer,J., Jones,D.T. *et al.* (2014) Classification of intrinsically disordered regions and proteins. *Chem. Rev.*, **114**, 6589–6631.
66. Orellana,L., Gustavsson,J., Bergh,C., Yoluk,O. and Lindahl,E. (2019) eBDIMS server: protein transition pathways with ensemble analysis in 2D-motion spaces. *Bioinformatics*, **35**, 3505–3507.
67. Ashwell,G. (1962) Enzymes of glucuronic and galacturonic acid metabolism in bacteria. In: Colowick,SP. and Kaplan,N.O. (eds). *Methods in Enzymology*. Academic Press, Cambridge, Massachusetts, Vol. **5**, pp. 190–208.
68. Hugouvieux-Cotte-Pattat,N. and Robert-Baudouy,J. (1983) Regulation of expression of the uxu operon and of the uxuR regulatory gene in *escherichia coli* K12. *Microbiology (Reading, Engl.)*, **129**, 3345–3353.
69. Yoon,S.H., Moon,T.S., Iranpour,P., Lanza,A.M. and Prather,K.J. (2009) Cloning and characterization of uronate dehydrogenases from two pseudomonads and *Agrobacterium tumefaciens* strain C58. *J. Bacteriol.*, **191**, 1565–1573.
70. Zhang,F., Carothers,J. and Keasling,J. (2012) Design of a dynamic sensor-regulator system for production of chemicals and fuels derived from fatty acids. *Nat. Biotechnol.*, **30**, 354–359
71. Doong,S.J., Gupta,A. and Prather,K.L.J. (2018) Layered dynamic regulation for improving metabolic pathway productivity in *Escherichia coli*. *Proc. Natl Acad. Sci. U.S.A.*, **12**. 2964–2969
72. Sakuta,R. and Nakamura,N. (2019) Production of hexaric acids from biomass. *Int. J. Mol. Sci.*, **20**, 3660.
73. Rodionova,I.A., Scott,D.A., Grishin,N.V., Osterman,A.L. and Rodionov,D.A. (2012) Tagaturonate–fructuronate epimerase UxaE, a novel enzyme in the hexuronate catabolic network in *Thermotoga maritima*. *Environ. Microbiol.*, **14**, 2920–2934.